

Magnetic nozzle and plasma detachment model for a steady-state flow

Cite as: Phys. Plasmas **15**, 057103 (2008); <https://doi.org/10.1063/1.2903844>

Submitted: 15 November 2007 . Accepted: 10 March 2008 . Published Online: 17 April 2008

B. N. Breizman, M. R. Tushentsov, and A. V. Arefiev



View Online



Export Citation

ARTICLES YOU MAY BE INTERESTED IN

[On plasma detachment in propulsive magnetic nozzles](#)

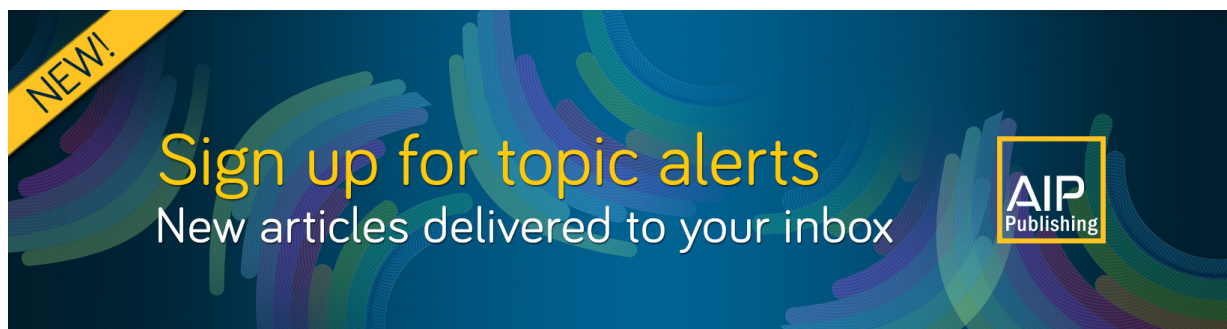
Physics of Plasmas **18**, 053504 (2011); <https://doi.org/10.1063/1.3589268>

[Two-dimensional supersonic plasma acceleration in a magnetic nozzle](#)

Physics of Plasmas **17**, 073501 (2010); <https://doi.org/10.1063/1.3442736>

[Magnetohydrodynamic scenario of plasma detachment in a magnetic nozzle](#)

Physics of Plasmas **12**, 043504 (2005); <https://doi.org/10.1063/1.1875632>

A banner with a dark blue background and colorful, abstract, swirling lines. In the top left corner, there is a yellow diagonal banner with the word "NEW!" in black. The main text in the center reads "Sign up for topic alerts" in a large, bold, yellow font, followed by "New articles delivered to your inbox" in a smaller, white font. In the bottom right corner, there is a white box containing the "AIP Publishing" logo.

NEW!

Sign up for topic alerts
New articles delivered to your inbox

AIP
Publishing

Magnetic nozzle and plasma detachment model for a steady-state flow^{a)}

B. N. Breizman,^{b)} M. R. Tushentsov, and A. V. Arefiev
The University of Texas at Austin, Austin, Texas 78712, USA

(Received 15 November 2007; accepted 10 March 2008; published online 17 April 2008)

Plasma propulsion concepts that employ a guiding magnetic field raise the question of how the magnetically controlled plasma can detach from the spacecraft. This paper presents a detachment scenario relevant to high-power thrusters in which the plasma can stretch the magnetic field lines to infinity, similar to the solar wind. In previous work, the corresponding ideal magnetohydrodynamics equations have been solved analytically for a plasma flow in a slowly diverging nozzle. That solution indicates that efficient detachment is feasible if the nozzle is sufficiently long. In order to extend the previous model beyond the idealizations of analytical theory, a Lagrangian code is developed in this work to simulate steady-state kinetic plasma flows and to evaluate nozzle efficiency. The code is benchmarked against the analytical results and then used to examine situations that are not analytically tractable, including plasma behavior in the recent Detachment Demonstration Experiment at the National Aeronautics and Space Administration. © 2008 American Institute of Physics. [DOI: 10.1063/1.2903844]

I. INTRODUCTION

An important feature of some high-power plasma thrusters is the presence of a strong guiding magnetic field. The magnetic field directs the plasma flow axially and prevents it from expanding radially towards the thruster walls. The use of a strong magnetic field brings up the issue of plasma detachment.^{1,2} The plasma flow may not be able to break free from the thruster to produce thrust, because the field lines generated by the thruster magnets are closed. As shown in Refs. 3 and 4, this issue can be resolved in the framework of ideal magnetohydrodynamics (MHD) by accelerating the flow to super-Alfvénic velocities within a magnetic nozzle. In a super-Alfvénic flow, the ion kinetic energy density exceeds the magnetic field energy density. As a result, the super-Alfvénic flow can change the configuration of the applied magnetic field.

In the magnetohydrodynamic detachment scenario, the outgoing super-Alfvénic flow detaches from the thruster together with the magnetic field. The magnetic field lines remain frozen into the plasma, as the flow stretches them to infinity. The magnetic field in the plume is almost entirely due to the plasma currents. It must be pointed out that this scenario mimics what occurs in the solar wind as it moves away from the Sun.⁵

In an initial attempt to describe the detachment quantitatively, an analytical solution of the ideal MHD equations was constructed in Ref. 4 for a plasma flow in a slowly diverging nozzle. The solution exhibits a well-behaved transition from sub- to super-Alfvénic flow inside the nozzle. Outside of the nozzle, the super-Alfvénic plume consists of two distinct parts: an unperturbed main flow with straight magnetic field lines and a rarefaction wave at the edge of the main flow. It is also shown in Ref. 4 that efficient detachment is feasible if the nozzle is sufficiently long.

The purpose of this paper is to generalize the detachment model of Ref. 4 to the case of kinetic ions and to develop a numerical procedure that could serve as a design tool to evaluate and optimize nozzle efficiency. This procedure is intended to be applicable to such plasma thrusters as variable specific impulse magnetoplasma rocket (VASIMR).⁶ In particular, it enables modeling of plasma detachment together with adiabatic transformation of ion gyromotion into directed energy of the plasma jet.

In our generalized model, the incoming plasma ions are assumed to have an anisotropic velocity distribution function, whereas plasma electrons are cold. These assumptions reflect essential features of the VASIMR concept. In the case of VASIMR, the incoming plasma flow is produced by an ion cyclotron resonance heating (ICRH) module that deposits rf power directly into the ion gyromotion. The ion cyclotron heating makes the ion velocity distribution anisotropic, with the ion gyroenergy significantly exceeding the energy of the axial motion. The plasma flow entering the ICRH module typically has a significant spread in the ion axial velocities. This spread may translate into a spread in the ion gyroenergies depending on specific conditions of single-pass ICRH scheme.^{7,8} The cold ion approximation used in Ref. 4 is only applicable to the case of a sufficiently small ion velocity spread. Other regimes require a fully kinetic treatment of the ions. To make the extended model flexible, we allow for an arbitrary ion distribution function in the incoming flow.

This work deals with a steady-state flow that establishes in the nozzle over time if the incoming ion distribution is kept constant. In a steady-state flow, the energy and the magnetic moment of a single ion are conserved. The incoming ion distribution written in terms of these variables remains constant along the magnetic field lines. Therefore, the problem reduces to finding the equilibrium magnetic field created by external coils together with a self-consistent plasma current that is a functional of the magnetic field itself.

We limit our analysis to paraxial (slowly diverging)

^{a)}Paper TI2 5, Bull. Am. Phys. Soc. 52, 276 (2007).

^{b)}Invited speaker.

flows, since this feature is required to achieve reasonable nozzle efficiencies.⁴ In Sec. II, we formulate a corresponding set of simplified basic equations, which we later solve numerically. The paraxial approximation enables us to precalculate the external magnetic field at the plasma-vacuum interface and to use an iterative procedure, if necessary, for a more accurate calculation of the vacuum field. Being designed to simulate steady-state flows directly, our numerical procedure appears to be more efficient than calculations based on time-dependent algorithms,¹¹ because the latter involve an additional dimension (time) and have to deal with transient phenomena.

Our simulations employ a Lagrangian radial grid associated with magnetic flux surfaces in the plasma. An important advantage of this grid is that it makes it particularly easy to trace the plasma-vacuum interface and to implement the corresponding boundary condition.¹² This grid is also convenient because the plasma radius increases considerably downstream from the nozzle exit.

We benchmark our code against the analytical results of Ref. 4 for the rarefaction wave at the edge of the plasma plume. We then present more examples of plasma flows, including an initial attempt to model the plasma plume in a recent detachment demonstration experiment at the National Aeronautics and Space Administration's Marshall Space Flight Center.^{9,10}

It is appropriate to point out that plasma flow in magnetic nozzles has received considerable attention in the past modeling efforts. This includes significant work associated with theta pinches and magnetoplasma dynamic (MPD) thrusters.^{12,13} A commonly accepted approach to such modeling is based on the MHD equations with either collision dominated or phenomenological transport coefficients. This approach implies a short mean free path for the plasma particles, which is typically not the case in the detachment problem because the plasma density decreases rapidly in the diverging nozzle. The detachment problem then requires a systematic kinetic treatment, especially when the ions in the incoming flow are strongly anisotropic. The kinetic description of ions is one of the distinctive aspects of the present paper. In general, electrons would also need to be treated kinetically to account for the electron pressure effects. This raises the question of calculating the electron distribution function together with a self-consistent ambipolar electric field, a problem that will be addressed independently in a separate paper. The electron physics is an intrinsic part of the incoming flow formation. In particular, it determines the transition from subsonic to supersonic flow due to ambipolar acceleration. However, when the flow is strongly supersonic, the electron pressure is naturally less important than the dynamical pressure of ions, and the same argument applies to the ambipolar electric field. The role of the electric field is also insignificant when the ions are energized via ICRH rather than via electron heating and subsequent ambipolar acceleration. It is therefore relevant to neglect the electron pressure and the electric field effects in solving the detachment problem for a given incoming supersonic flow, which simplifies the problem a great deal while capturing the important role of sub- to super-Alfvénic transition.

II. BASIC EQUATIONS

We start with Vlasov–Maxwell equations for an axisymmetric steady-state flow of collisionless plasma. We consider a preformed supersonic plasma flow that consists of energetic ions and cold electrons and assume the absence of plasma rotation; i.e., the absence of $E \times B$ drift. Under the above assumptions the electric field in plasma can be neglected (the absence of the parallel electric field results from high electron conductivity along the magnetic field lines, whereas the absence of the transverse electric field reflects the absence of plasma rotation). The resulting steady-state Vlasov equation for the ion distribution function f_i has the form

$$m_i \mathbf{v}_i \cdot \nabla f_i + \frac{q_i}{c} [\mathbf{v}_i \times \mathbf{B}] \cdot \nabla f_i = 0. \quad (1)$$

The Vlasov equation for cold electrons with zero inertia is

$$\frac{q_e}{c} [\mathbf{v}_e \times \mathbf{B}] \cdot \nabla f_e = 0. \quad (2)$$

The Maxwell equations require that the magnetic field \mathbf{B} is divergence free,

$$\nabla \cdot \mathbf{B} = 0, \quad (3)$$

and that the field is related to the plasma current by Ampère's law:

$$\mathbf{j} = \frac{c}{4\pi} \nabla \times \mathbf{B}. \quad (4)$$

In what follows, we assume that the magnetic field has only two components (axial and radial) in our axisymmetric problem. The corresponding plasma current has only one (azimuthal) component.

We find from Eq. (2) that the cold electrons have no macroscopic velocity (carry no current) across the magnetic field. The cross-field current is then carried only by ions, so that

$$\mathbf{j}_\perp = q_i \int f_i \mathbf{v}_\perp d^3v. \quad (5)$$

Equations (1)–(5) apparently conserve momentum, as expressed by the following momentum balance relation:

$$\frac{\partial}{\partial x_\beta} \left(\Pi_{\alpha\beta} + \frac{B^2}{8\pi} \delta_{\alpha\beta} - \frac{B_\alpha B_\beta}{4\pi} \right) = 0, \quad (6)$$

where

$$\Pi_{\alpha\beta} \equiv m_i \int v_\alpha v_\beta f_i d^3v \quad (7)$$

is the ion momentum flux tensor that includes both the flux associated with the directed flow and the flux associated with the ion velocity spread (ion pressure). Assuming that the ions are magnetized, so that their Larmor radii remain much smaller than the plasma radius, we evaluate the ion momentum flux tensor by using a gyroaveraged distribution function defined as

$$\langle f_i \rangle \equiv \frac{1}{2\pi} \int_0^{2\pi} f_i d\psi, \quad (8)$$

where ψ is the gyroangle in the velocity space. In this limit, we have

$$\Pi_{\alpha\beta} = \Pi_{\perp} \delta_{\alpha\beta} + (\Pi_{\parallel} - \Pi_{\perp}) b_{\alpha} b_{\beta}, \quad (9)$$

where $\mathbf{b} \equiv \mathbf{B}/|\mathbf{B}|$ is the unit vector in the direction of the local magnetic field and

$$\Pi_{\perp} \equiv \frac{m_i}{2} \int v_{\perp}^2 \langle f_i \rangle d^3v, \quad (10)$$

$$\Pi_{\parallel} \equiv m_i \int v_{\parallel}^2 \langle f_i \rangle d^3v. \quad (11)$$

The structure of the momentum flux tensor suggests splitting Eq. (6) into two components [parallel and perpendicular to the magnetic field line in the $(r; z)$ plane of the cylindrical coordinate system]. The third (azimuthal) component of the equation vanishes automatically due to the axial symmetry of the problem. We thus obtain

$$(\mathbf{b} \cdot \nabla) \Pi_{\parallel} + (\Pi_{\parallel} - \Pi_{\perp})(\nabla \cdot \mathbf{b}) = 0, \quad (12)$$

$$\nabla_{\perp} \left(\Pi_{\perp} + \frac{B^2}{8\pi} \right) + \left(\Pi_{\parallel} - \Pi_{\perp} - \frac{B^2}{4\pi} \right) (\mathbf{b} \cdot \nabla) \mathbf{b} = 0. \quad (13)$$

The function $\langle f_i \rangle$ in the expressions (10) and (11) for Π_{\perp} and Π_{\parallel} satisfies a gyroaveraged Vlasov equation known from the lowest order guiding center theory¹⁴

$$m_i v_{\parallel} b_{\alpha} \frac{\partial \langle f_i \rangle}{\partial x_{\alpha}} = 0, \quad (14)$$

which simply means that, for any fixed values of the ion energy $\varepsilon \equiv m_i(v_{\perp}^2 + v_{\parallel}^2)/2$ and magnetic moment $\mu \equiv m_i v_{\perp}^2/2B$, this function is constant along the magnetic field lines. Therefore, in the axisymmetric magnetic field, $\langle f_i \rangle$ is an arbitrary function of ε , μ and a , where a is the flux surface label. This function specifies properties of the incoming plasma flow and it serves as an input function in our problem. This lowest order solution is apparently independent of gyrophase. As a result, it does not contribute to the ion current defined by Eq. (5). The ion current is determined by the small gyrophase-dependent corrections to the distribution function, associated with the curvature drift and the diamagnetic drift. These small current-carrying corrections can be safely neglected in expressions (10) and (11) for the momentum flux tensor.

Once the function $\langle f_i \rangle$ is specified, the problem reduces to finding the profiles of B_r and B_z from Eqs. (3), (12), and (13). It may seem that this set of equations is overdetermined because we have three scalar equations for the two unknown functions B_r and B_z . However, only two of these three equations are, in fact, independent because Eq. (12) is satisfied automatically due to Eq. (14). In order to demonstrate that, we change integration variables in expressions (10) and (11) from v_{\perp} and v_{\parallel} to ε and μ ; i.e.,

$$dv_{\perp}^2 dv_{\parallel} = \frac{2B}{m_i^2} \left(\frac{2(\varepsilon - \mu B)}{m_i} \right)^{-1/2} d\mu d\varepsilon. \quad (15)$$

Substituting the expressions (10) and (11) for Π_{\perp} and Π_{\parallel} into Eq. (12), we obtain

$$\begin{aligned} & (\mathbf{b} \cdot \nabla) \Pi_{\parallel} + (\Pi_{\parallel} - \Pi_{\perp})(\nabla \cdot \mathbf{b}) \\ &= m_i \int (\mathbf{b} \cdot \nabla) \langle f_i \rangle (a, \mu, \varepsilon) \\ & \quad \times 2\pi \frac{2B}{m_i^2} \left(\frac{2(\varepsilon - \mu B)}{m_i} \right)^{1/2} d\mu d\varepsilon. \end{aligned} \quad (16)$$

This expression apparently vanishes because the gyroaveraged distribution function is constant along the magnetic field lines as required by Eq. (14). Given that Eq. (12) resolves the compatibility issue for Eqs. (3), (12), and (13), one can drop Eq. (12), provided that Π_{\perp} and Π_{\parallel} are calculated from Eqs. (10) and (11) with a function $\langle f_i \rangle$ that satisfies Eq. (14). However, it appears to be more attractive from the numerical standpoint to calculate just one of the quantities Π_{\perp} or Π_{\parallel} and then solve the set of all three equations to determine B_r , B_z , and the remaining component of the pressure tensor. An obvious benefit of the second approach is that only one of the two velocity space integrations needs to be performed by the code at every spatial location.

Our numerical procedure for solving Eqs. (3), (12), and (13) is tailored to the case of most interest in terms of practical applications. It is designed to model a nozzle that produces a well-directed plasma flow. The latter implies that the radial component of the magnetic field in the plasma is much smaller than the axial component of the field. It also implies that the plasma flow is highly super-Alfvénic at the nozzle exit. Violation of any of these two conditions will clearly degrade the nozzle efficiency. Our goal then is to ensure that the model is sufficiently accurate in the regimes where both conditions are satisfied. This will allow us to quantify the nozzle efficiency in the most relevant parameter range. Our model will be less accurate at low efficiencies, but these regimes are of little interest anyway. Yet, even without being quantitative with regard to inefficient nozzles, the model can still serve as an indicator of what parameter range to avoid.

Guided by these thoughts, we simplify Eq. (13) by neglecting the term $(\Pi_{\perp} + B^2/4\pi)(\mathbf{b} \cdot \nabla) \mathbf{b}$ compared to $\nabla_{\perp}(\Pi_{\perp} + B^2/8\pi)$, as we assume that the radial spatial scale is much shorter than the axial scale in a well-directed flow. We still keep the term $\Pi_{\parallel}(\mathbf{b} \cdot \nabla) \mathbf{b}$ in this equation because the parallel component of the momentum flux tensor exceeds $B^2/8\pi$ in a highly super-Alfvénic flow. Moreover, the term $\Pi_{\parallel}(\mathbf{b} \cdot \nabla) \mathbf{b}$ eventually becomes the dominant one in Eq. (13) as both the magnetic pressure and Π_{\perp} decrease downstream faster than Π_{\parallel} . The fast decrease of Π_{\perp} results from the conservation of magnetic moment for magnetized ions. An additional relevant approximation is to replace B^2 by B_z^2 in all expressions, because the radial component of the magnetic field gives only a second-order correction to B^2 in our problem of interest. As a result of the described approximations, we finally obtain the following simplified set of basic equations in cylindrical coordinates:

$$\left(\frac{\partial}{\partial z} + \frac{B_r}{B_z} \frac{\partial}{\partial r}\right) B_z = -B_z \frac{1}{r} \frac{\partial}{\partial r} \left(r \frac{B_r}{B_z}\right), \quad (17)$$

$$\left(\frac{\partial}{\partial z} + \frac{B_r}{B_z} \frac{\partial}{\partial r}\right) \Pi_{\parallel} = -(\Pi_{\parallel} - \Pi_{\perp}) \frac{1}{r} \frac{\partial}{\partial r} \left(r \frac{B_r}{B_z}\right), \quad (18)$$

$$\left(\frac{\partial}{\partial z} + \frac{B_r}{B_z} \frac{\partial}{\partial r}\right) \frac{B_r}{B_z} = -\frac{1}{\Pi_{\parallel}} \frac{\partial}{\partial r} \left(\Pi_{\perp} + \frac{B_z^2}{8\pi}\right), \quad (19)$$

$$\begin{aligned} \Pi_{\perp} = \frac{m_i}{2} \int \langle f_i \rangle (a, \mu, \varepsilon) \frac{2\mu B_z}{m_i} \\ \times 2\pi \frac{2B_z}{m_i^2} \left(\frac{2(\varepsilon - \mu B_z)}{m_i}\right)^{-1/2} d\mu d\varepsilon. \end{aligned} \quad (20)$$

Here, $\langle f_i \rangle$ is a given input function of its arguments and $a(r; z)$ is the magnetic flux surface label that is constant along the field lines,

$$\left(\frac{\partial}{\partial z} + \frac{B_r}{B_z} \frac{\partial}{\partial r}\right) a = 0, \quad (21)$$

and which will serve as the Lagrangian radial coordinate in our code.

Equations (17)–(19) reduce to paraxial ideal MHD equations with anisotropic pressure if all ions on a given magnetic flux surface have the same energy ε_* and the same magnetic moment μ_* , such that

$$\langle f_i \rangle = F \delta(\mu - \mu_*) \delta(\varepsilon - \varepsilon_*), \quad (22)$$

where the quantities F , ε_* , and μ_* are functions of the flux surface label a . In this case, the flow velocity is just v_{\parallel} . We use the approximation $B \approx B_z$ to find from the ion energy conservation such that

$$v_{\parallel} = \sqrt{\frac{2}{m_i} (\varepsilon_* - \mu_* B_z)}. \quad (23)$$

Integration of the distribution function (22) over the entire velocity space and subsequent replacement of B by B_z yield the ion density,

$$n_i = F \frac{4\pi B_z}{m_i^2 v_{\parallel}}. \quad (24)$$

We next use Eqs. (10) and (11) together with the approximation $B \approx B_z$ to find that

$$\Pi_{\perp} = n_i \mu_* B_z, \quad (25)$$

$$\Pi_{\parallel} = n_i m_i v_{\parallel}^2. \quad (26)$$

There is no need to use Eq. (18) any longer, because Eq. (26) gives an explicit expression for Π_{\parallel} . Taking into account expressions (25) and (26), we transform Eq. (19) into

$$\left(\frac{\partial}{\partial z} + \frac{B_r}{B_z} \frac{\partial}{\partial r}\right) \frac{B_r}{B_z} = -\frac{1}{n_i m_i v_{\parallel}^2} \frac{\partial}{\partial r} \left(n_i \mu_* B_z + \frac{B_z^2}{8\pi}\right). \quad (27)$$

Equations (17) and (27), together with the expressions for n_i and v_{\parallel} [Eqs. (24) and (23)], determine the self-consistent configuration of a paraxial magnetic field in the plasma flow.

In the absence of gyromotion, this set of equations is equivalent to the paraxial MHD description presented in Ref. 4.

III. MAGNETIC FIELD OUTSIDE THE PLASMA

As already pointed out, our goal is to simulate a well directed plasma flow, which implies that the field lines in the plasma are paraxial (both inside the nozzle and in the outgoing plasma plume). This regime requires the guiding magnetic field generated by the external coils to be paraxial inside the nozzle. However, the field lines are not necessarily paraxial in the vacuum region outside the plasma plume. This vacuum magnetic field is essential to our problem because it determines the boundary condition at the plasma-vacuum interface.

In general, the location of the plasma boundary needs to be found self-consistently, which couples the equations for magnetic field in the plasma to the equations for the vacuum field. However, the specific features of our problem suggest an efficient iterative procedure to calculate the vacuum magnetic field.

The initial step is to calculate the vacuum magnetic field for a given configuration of the external coils under the assumption that the plasma is a perfectly conducting cylinder with radius r_p . The radial component of the vacuum magnetic field then vanishes at $r=r_p$. This approach is justified by the fact that the flow diverges slowly compared to the vacuum magnetic field that comes out of the nozzle. We describe the axisymmetric vacuum magnetic field \mathbf{B} in terms of a vector potential $\mathbf{A} = A \mathbf{e}_{\phi}$, with

$$B_r = -\frac{\partial A}{\partial z}, \quad (28)$$

$$B_z = \frac{1}{r} \frac{\partial}{\partial r} (rA). \quad (29)$$

The corresponding equation for A is given by

$$\nabla^2 A - \frac{A}{r^2} = -\frac{4\pi}{c} j_c, \quad (30)$$

where j_c is the azimuthal current density in the coils.

To solve Eq. (30), we choose a computational box with $z_{\min} \leq z \leq z_{\max}$ and $r_p \leq r \leq r_{\max}$ and impose the following boundary conditions:

$$A(r, z_{\min}) = A(r, z_{\max}) = A(r_{\max}, z) = 0, \quad (31)$$

$$A(r_p, z) = 0. \quad (32)$$

The values of r_{\max} , z_{\max} , and $|z_{\min}|$ must be sufficiently large to minimize the effect of the computational box. If the radius of the magnetic coils is comparable to r_p , then it is necessary to have $r_{\max} \gg r_p$. The distances from the nozzle entrance and the nozzle exit to the end walls of the computational box must be also much greater than r_p .

Solving Eq. (30) numerically with the boundary conditions (31) and (32), we find $A(r_p, z)$. We then use this function and Eq. (29) to find $B_z(r_p, z)$, which is the lowest order expression for the magnetic field at the plasma-vacuum interface. The next step now is to solve the plasma equations

using this magnetic field as a boundary condition. This solution gives us the magnetic field in the plasma together with a corrected location of the plasma boundary $r_p(z)$.

The initial step presents a good approximation for the vacuum magnetic field outside a slowly diverging flow. The knowledge of the plasma boundary allows us to continue iterations. The only modification to the previous procedure is in the boundary location. We have to replace Eq. (32) with $A[r_p(z), z]=0$. We also need to continue the solution upstream from the nozzle entrance to $z=z_{\min}$, because the plasma equations are solved only downstream from the nozzle entrance ($z>0$). The following condition can be used to achieve this: $A[r_p(0), z]=0$ for $z_{\min} \leq z \leq 0$.

The described iterative procedure can be continued to achieve desired precision. In what follows, we limit ourselves only to the first step. It turns out to be sufficient for practical purposes.

IV. LAGRANGIAN FORMULATION AND NUMERICAL SCHEME

It is convenient to switch from (r, z) to new variables (a, z) , where a is a coordinate labeling magnetic flux surfaces. We define a as the magnetic flux surface radius in the incoming flow, such that $a=r$ at $z=0$ and $a \in [0; r_p]$, where r_p is the plasma radius in the incoming flow. Equation (21) indicates that the differential operator $[\partial/\partial z + (B_r/B_z)(\partial/\partial r)]$ in Eqs. (17)–(19) is the derivative along the magnetic flux surfaces; i.e.,

$$\frac{\partial}{\partial z} \Big|_r + \frac{B_r}{B_z} \frac{\partial}{\partial r} \Big|_z = \frac{\partial}{\partial z} \Big|_a. \quad (33)$$

The conservation of magnetic flux, i.e., $2\pi r B_z dr = 2\pi a B_{z0} da$, readily yields the following relation:

$$\frac{\partial}{\partial r} \Big|_z = \frac{r B_z}{a B_{z0}} \frac{\partial}{\partial a} \Big|_z, \quad (34)$$

where B_{z0} is the axial magnetic field in the incoming flow. We now use expressions (33) and (34) to transform Eqs. (17)–(19) into

$$\left(\frac{\partial B_z}{\partial z} \right)_a = - \frac{B_z^2}{a B_{z0}} \left[\frac{\partial}{\partial a} \left(r \frac{B_r}{B_z} \right) \right]_z, \quad (35)$$

$$\left(\frac{\partial \Pi_{\parallel}}{\partial z} \right)_a = - (\Pi_{\parallel} - \Pi_{\perp}) \frac{B_z}{a B_{z0}} \left[\frac{\partial}{\partial a} \left(r \frac{B_r}{B_z} \right) \right]_z, \quad (36)$$

$$\left[\frac{\partial}{\partial z} \left(\frac{B_r}{B_z} \right) \right]_a = - \frac{1}{\Pi_{\parallel}} \frac{r B_z}{a B_{z0}} \left[\frac{\partial}{\partial a} \left(\Pi_{\perp} + \frac{B_z^2}{8\pi} \right) \right]_z. \quad (37)$$

We must also add an equation for r , since r explicitly enters Eqs. (35)–(37). The equation for r ,

$$\left(\frac{\partial r}{\partial z} \right)_a = \frac{B_r}{B_z}, \quad (38)$$

results from comparing Eq. (33) with an expression for $(\partial/\partial z)_a$ that describes the transformation of variables,

$$\frac{\partial}{\partial z} \Big|_a = \frac{\partial}{\partial z} \Big|_r + \left(\frac{\partial r}{\partial z} \right)_a \frac{\partial}{\partial r} \Big|_z. \quad (39)$$

A closed system of equations consists of Eqs. (35)–(38) and Eq. (20) for Π_{\perp} . Equations (35)–(38) have the structure of one-dimensional evolution equations for the unknown functions B_z , Π_{\parallel} , B_r/B_z , and r . We thereby reduce our steady-state problem to an initial value problem for Eqs. (35)–(38), with the coordinate z playing the role of time.

We use two staggered grids in the computational domain $a \in [0, r_p]$ to discretize the quantities B_z , Π_{\parallel} , Π_{\perp} , B_r/B_z , and r . The main grid consists of equally spaced points with coordinates $a_k = \Delta a(k-1)$, where $k \in [1; N]$ is an integer and $\Delta a = r_p/(N-1/2)$ is the distance between the grid points. The secondary grid consists of “half-integer” points with coordinates $a_{k+1/2} = \Delta a(k-1/2)$. By definition, we have $a_1 = 0$ and $a_{N+1/2} = r_p$. The quantities (B_r/B_z) and r are defined on the main grid, whereas the quantities B_z , Π_{\parallel} , and Π_{\perp} are defined on the secondary grid. This discretization, which is motivated by the structure of Eqs. (35)–(38), follows the idea of the Yee scheme.¹⁵ The finite difference equations corresponding to Eqs. (35)–(38) have the following form:

$$\begin{aligned} \frac{\partial}{\partial z} (B_z)_{k+1/2} = & - \frac{(B_z^2)_{k+1/2}}{a_{k+1/2} (B_{z0})_{k+1/2} \Delta a} \\ & \times \left[r_{k+1} \left(\frac{B_r}{B_z} \right)_{k+1} - r_k \left(\frac{B_r}{B_z} \right)_k \right], \end{aligned} \quad (40)$$

$$\begin{aligned} \frac{\partial}{\partial z} (\Pi_{\parallel})_{k+1/2} = & \frac{(B_z)_{k+1/2} [(\Pi_{\perp})_{k+1/2} - (\Pi_{\parallel})_{k+1/2}]}{a_{k+1/2} (B_{z0})_{k+1/2} \Delta a} \\ & \times \left[r_{k+1} \left(\frac{B_r}{B_z} \right)_{k+1} - r_k \left(\frac{B_r}{B_z} \right)_k \right], \end{aligned} \quad (41)$$

$$\begin{aligned} \frac{\partial}{\partial z} \left(\frac{B_r}{B_z} \right)_k = & - \frac{r_k}{2a_k \Delta a} \left[\frac{(B_z)_{k+1/2}}{(\Pi_{\parallel})_{k+1/2} (B_{z0})_{k+1/2}} \right. \\ & \left. + \frac{(B_z)_{k-1/2}}{(\Pi_{\parallel})_{k-1/2} (B_{z0})_{k-1/2}} \right] \\ & \times \left[(\Pi_{\perp})_{k+1/2} + \frac{1}{8\pi} (B_z^2)_{k+1/2} - (\Pi_{\perp})_{k-1/2} \right. \\ & \left. - \frac{1}{8\pi} (B_z^2)_{k-1/2} \right], \end{aligned} \quad (42)$$

$$\frac{\partial r_k}{\partial z} = \left(\frac{B_r}{B_z} \right)_k. \quad (43)$$

The index k runs from 1 to $(N-1)$ in Eqs. (40) and (41) and from 2 to N in Eqs. (42) and (43).

An important feature of the staggered grids is that Eqs. (40) and (41) only involve inner boundary conditions and Eq. (42) only involves outer boundary conditions.

The inner boundary conditions that we use with Eqs. (40) and (41) are

$$r_1 = a_1 = 0, \quad (44)$$

$$\left(\frac{B_r}{B_z}\right)_1 = 0. \quad (45)$$

The outer boundary condition is the conservation of the transverse momentum flux:

$$(\Pi_\perp)_{N+1/2} + \frac{1}{8\pi}(B_z^2)_{N+1/2} = \frac{1}{8\pi}[B_z^{\text{vac}}(z)]^2, \quad (46)$$

where $B_z^{\text{vac}}(z)$ is the axial component of the vacuum magnetic field at the plasma boundary. The function $B_z^{\text{vac}}(z)$ is assumed to be computed independently using the procedure described in Sec. III. Since Π_\perp is a functional of B_z , Eq. (46) is essentially an equation for B_z inside the plasma near the plasma-vacuum interface. Equation (42) requires not only the quantities determined by Eq. (46), but also $(\Pi_\parallel)_{N+1/2}$ and $(B_z)_{N+1/2}$. The value of $(B_z)_{N+1/2}$ is known from the “initial” flow configuration. The value of $(\Pi_\parallel)_{N+1/2}$ must be calculated from Eq. (11) using the value of $(B_z)_{N+1/2}$ found by solving Eq. (46).

The system of equations (40)–(43) is solved using the explicit Runge–Kutta(2,3) solver (Bogacki–Shampine pair)¹⁶ that is more effective than the standard fourth-order Runge–Kutta solver, given the presence of mild stiffness in Eqs. (40)–(43).

V. CODE BENCHMARKING AND SIMULATION RESULTS

A. Benchmarking

To benchmark the code, we consider a highly super-Alfvénic flow of a cold plasma that comes out of a conical magnetic nozzle. The analytical solution for the case without a vacuum gap between the plasma and the nozzle wall is presented in Ref. 4. We use our code to simulate a similar regime and compare the numerical results with the analytical solution.

We start by reviewing the analytical solution. In an infinitely long conical nozzle with a perfectly conducting wall located at $r(z) = z \tan \theta_0$, the magnetic field lines are straight. The corresponding paraxial solution for $\theta_0 \ll 1$ is given by

$$B_z = \frac{2\Phi_0}{z^2 \theta_0^2}, \quad (47)$$

$$\frac{B_r}{B_z} = \frac{r}{z}, \quad (48)$$

where $2\pi\Phi_0$ is the total magnetic flux and θ_0 is the nozzle divergence angle (see Fig. 1). This solution satisfies Eqs. (17) and (27) for $\mu_* = 0$. The plasma motion is force free in the nozzle.

In the case of a finite-length conical nozzle, the solution inside the nozzle is still given by Eqs. (47) and (48), provided that the outgoing flow is highly super-Alfvénic and that there is no vacuum gap between the plasma and the nozzle wall. The plume consists of an unperturbed main flow [Eqs. (47) and (48)] and a rarefaction wave at the flow edge. The expression for the field in the rarefaction wave can be derived directly from Eqs. (17) and (27).

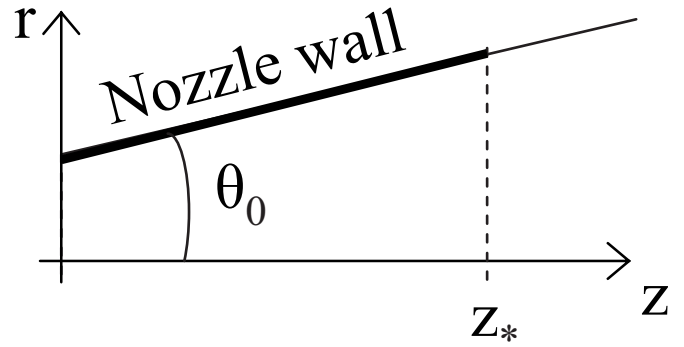


FIG. 1. Layout of a conical magnetic nozzle with a divergence angle θ_0 .

The rarefaction wave is localized in a thin layer near the plasma boundary. In the unperturbed main flow, we have $B_r/B_z = r/z$, as follows from Eq. (48). To find the solution in the rarefaction wave, we present B_r/B_z in the form

$$\frac{B_r}{B_z} = \frac{r}{z} + \delta\theta, \quad (49)$$

where r/z is essentially the slope of the magnetic field line without the rarefaction wave and $\delta\theta$ is a small correction associated with the wave. We use the definition (49) to rewrite Eqs. (17) and (27),

$$\left[\frac{\partial}{\partial z} + \left(\frac{r}{z} + \delta\theta \right) \frac{\partial}{\partial r} \right] B_z = -\frac{2B_z}{z} - B_z \frac{\partial}{\partial r} (\delta\theta) - B_z \frac{\delta\theta}{r}, \quad (50)$$

$$\left[\frac{\partial}{\partial z} + \left(\frac{r}{z} + \delta\theta \right) \frac{\partial}{\partial r} \right] \delta\theta = -\frac{\delta\theta}{z} - \frac{B_z}{4\pi n_i m_i v_\parallel^2} \frac{\partial B_z}{\partial r}. \quad (51)$$

The last term in Eq. (50) is much smaller than $B_z \partial(\delta\theta)/\partial r$, because $\delta\theta$ varies in a thin layer. We can therefore simplify Eq. (50) by neglecting this term. We also note that n_i/B_z and v_\parallel remain constant along the magnetic field lines [see Eqs. (23) and (24)], so that

$$\frac{B_z}{4\pi n_i m_i v_\parallel^2} = \frac{1}{B_* M_A^2} \quad (52)$$

is a constant quantity as well, where $B_* \equiv 2\Phi_0/z_*^2 \theta_0^2$ and $M_A \equiv [v_\parallel / \sqrt{B_z^2/4\pi m_i n_i}]_{z=z_*}$ are the magnetic field and the Alfvénic Mach number at the end of the nozzle located at $z = z_*$. Based on the above remarks, we transform Eqs. (50) and (51) into

$$\left[\frac{\partial}{\partial z} + \left(\frac{r}{z} + \delta\theta \right) \frac{\partial}{\partial r} \right] B_z = -\frac{2B_z}{z} - B_z \frac{\partial}{\partial r} (\delta\theta), \quad (53)$$

$$\left[\frac{\partial}{\partial z} + \left(\frac{r}{z} + \delta\theta \right) \frac{\partial}{\partial r} \right] \delta\theta = -\frac{\delta\theta}{z} - \frac{1}{B_* M_A^2} \frac{\partial B_z}{\partial r}. \quad (54)$$

The exact solution of these equations is

$$B_z = B_* \frac{z_*^2}{z^2} \begin{cases} 1, & r \leq r_c \\ \frac{1}{9} [M_A (\theta_0 z - r) + 2(z - z_*)]^2 (z - z_*)^{-2}, & r_c < r \leq r_{pv} \\ 0, & r_{pv} \leq r, \end{cases} \quad (55)$$

$$\delta\theta = \frac{2}{M_A} \left(\frac{z_*}{z} - \sqrt{\frac{B_z}{B_*}} \right), \quad (56)$$

where

$$r_{pv} \equiv z\theta_0 \left[1 + \frac{2}{\theta_0 M_A} \left(1 - \frac{z_*}{z} \right) \right] \quad (57)$$

is the location of the plasma-vacuum interface and

$$r_c \equiv z\theta_0 \left[1 - \frac{1}{\theta_0 M_A} \left(1 - \frac{z_*}{z} \right) \right] \quad (58)$$

is the location of the inner wave front. [The expression for r_c given here by Eq. (58) is slightly different from that given by Eq. (77) in Ref. 4. Equation (58) is a linear expansion of Eq. (77) with respect to the small parameter $1/\theta_0 M_A \ll 1$.] A plot of the solution given by Eq. (55) is shown in Fig. 2.

To simulate the conical nozzle shown in Fig. 1, with a divergence angle θ_0 and magnetic flux Φ_0 , we choose the magnetic field at the nozzle entrance ($z = z_{in}$) in accordance with Eqs. (47) and (48). Inside the nozzle, we impose the following magnetic field at the plasma boundary: $B = B(r_p, z_{in}) r_p^2 / z^2 \theta_0^2$, where r_p is the radius of the incoming plasma flow and $B(r_p, z_{in}) \equiv 2\Phi_0 / z^2 \theta_0^2$. Note that the axial coordinate z is defined such that the nozzle's wall is located

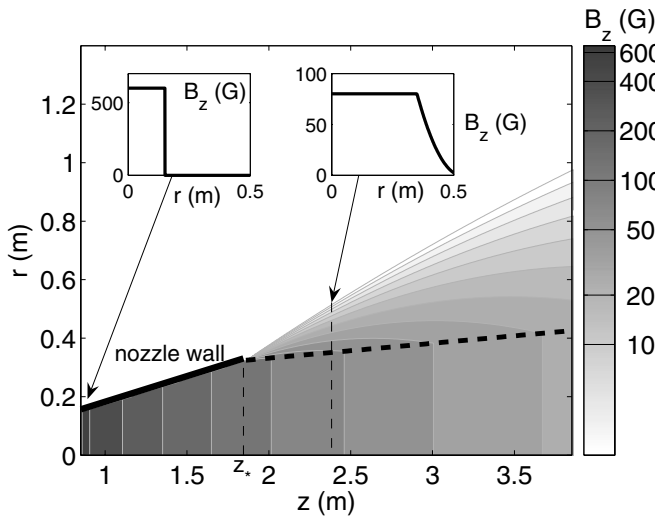


FIG. 2. Analytical solution for a highly super-Alfvénic cold plasma flow coming out of a conical magnetic nozzle with a divergence angle $\theta_0 = 10^\circ$ [Eqs. (55), (57), and (58)]. The end of the nozzle is located at $z_* = 1.87$ m. The contours show the levels of constant B_z , with the scale indicated on the sidebar. The insets give radial profiles of B_z in the incoming flow ($z = 0.87$ m) and in the plume ($z = 2.37$ m). The thick dashed line marks the inner front of the rarefaction wave $r_c(z)$ [see Eq. (58)]. The incoming flow parameters ($z = 0.87$ m) are $n_i = 5.0 \times 10^{20} \text{ m}^{-3}$, $\varepsilon_{||} = 250 \text{ eV}$, and $r_p = 0.15$ m.

at $r = \theta_0 z$. To simulate the rarefaction wave, we impose a sharply decreasing magnetic field at the plasma boundary downstream from the nozzle exit ($z > z_*$). The pattern of the rarefaction wave is insensitive to details of the decrease, as long as the field decreases with z much faster than $B(r_p, z_{in}) r_p^2 / z^2 \theta_0^2$. Figure 3 shows a well pronounced rarefaction wave at the plasma boundary. As expected, the central part of the flow remains unperturbed. The good agreement between Figs. 3 and 2 ensures that the code is reasonably accurate.

B. Numerical examples of plasma detachment

Simulations presented in this subsection involve transition from sub- to super-Alfvénic flow. The first example refers to cold ions with an initial velocity directed along the guiding magnetic field. We consider a cylindrical nozzle with a vacuum gap between the plasma and the nozzle wall. The magnetic coils represent a long (semi-infinite) solenoid with an inner radius of $R = 0.25$ m and with a uniform current distribution in the coils. The incoming plasma radius is $r_p = 0.15$ m. The ion energy in the incoming plasma flow is $\varepsilon_{||} = 10 \text{ eV}$, the incoming density is $n_{i0} = 5.0 \times 10^{20} \text{ m}^{-3}$. These parameters correspond to the power level of 395 kW for argon plasma. The magnetic field deep inside the nozzle is 600 G. Figure 4 shows the behavior of the Alfvénic Mach number M_A in the plasma jet. The thick solid line separates the sub- and super-Alfvénic regions in the plasma flow. The

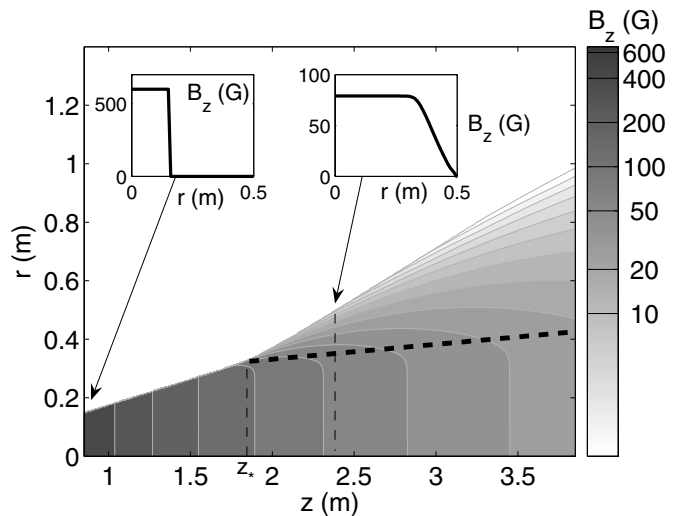


FIG. 3. Simulation results for a highly super-Alfvénic flow coming out of a conical magnetic nozzle. The nozzle divergence angle and the incoming flow parameters are the same as in Fig. 2. The thick dashed line marks the inner front of the rarefaction wave $r_c(z)$ in the analytical solution [see Eq. (58)].

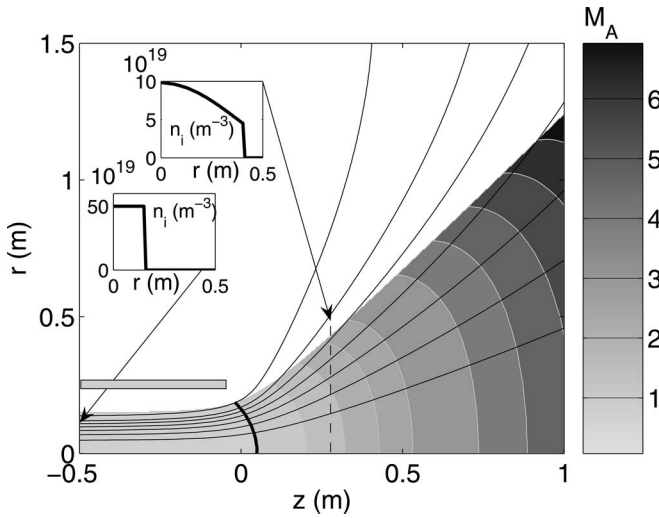


FIG. 4. Sub- to super-Alfvénic transition in the plume of a cylindrical nozzle. The contours show the levels of constant Alfvénic Mach number M_A , with the scale indicated on the sidebar. The thick solid line separates the sub- and super-Alfvénic regions in the cold plasma flow. The light gray bar marks the location of the solenoid coils and the thin solid lines are the magnetic field lines of the solenoid in the absence of plasma. The insets give radial profiles of n_i in the incoming flow ($z = -0.5$ m) and in the plume ($z = 0.25$ m).

sub- to super-Alfvénic transition occurs somewhat outside the solenoid close to its end. The shape of the shaded area in the plot shows that the plasma plume does not follow the vacuum magnetic field lines from the solenoid, which is a clear evidence of detachment. This conclusion also follows from calculations of detachment efficiency (see Sec. V C).

The second example demonstrates detachment together with conversion of ion gyroenergy into directed energy of the plasma jet. The nozzle is again a semi-infinite solenoid with the inner radius $R = 0.25$ m. The incoming plasma radius is $r_p = 0.1$ m and the incoming ion gyroenergy is $\varepsilon_\perp = 100$ eV, which is the same for all ions. The longitudinal energy is $\varepsilon_\parallel = 10$ eV without any spread in parallel velocities. The ion density is $n_0 = 5.0 \times 10^{20} \text{ m}^{-3}$. The corresponding power is 193 kW for argon plasma. A contour plot of the transverse-to-longitudinal energy ratio presented in Fig. 5 shows that the conversion of the ion gyroenergy into the energy of directed flow facilitates detachment. Note that the plasma plume has a very small divergence angle far away from the nozzle, where the ions are strongly super-Alfvénic and have almost no gyroenergy left.

C. Nozzle efficiency

The term “nozzle efficiency” requires some clarification when it is used as a quantitative characteristic. One can define efficiency in terms of power or in terms of thrust. A common definition of the power efficiency (η_p) is the ratio of the “directed” power in the plasma plume to the power in the incoming plasma flow, i.e.,

$$\eta_p = \left[\int f_\infty v_z v_z^2 d^3v d(\pi r^2) \right] \left[\int f_0 v_z v^2 d^3v d(\pi r^2) \right]^{-1}, \quad (59)$$

where f_0 and f_∞ , respectively, are the ion distribution functions at the nozzle entrance and in the plume, v_z is the axial

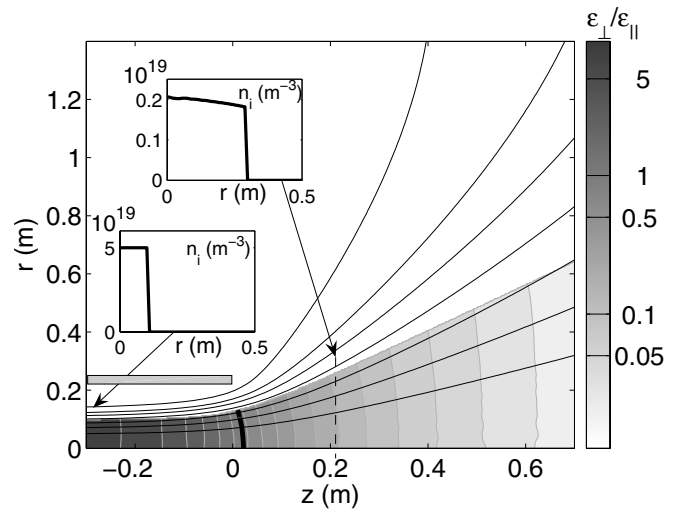


FIG. 5. Transition from sub- to super-Alfvénic flow with a simultaneous conversion of the ion gyroenergy ε_\perp into the axial energy ε_\parallel . The contours show the levels of constant $\varepsilon_\perp/\varepsilon_\parallel$ ratio. The thick solid line marks the location where $\varepsilon_\perp/\varepsilon_\parallel = 1$. The light gray bar marks the location of the solenoid coils and the thin solid lines are the magnetic field lines of the solenoid in the absence of plasma. The insets give radial profiles of n_i in the incoming flow ($z = -0.3$ m) and in the plume ($z = 0.21$ m).

component of the velocity, and the integration is performed over the velocity space and over the plasma cross section. The thrust efficiency η_T can be defined as a ratio of the momentum flux in the plume to the maximum axial momentum that a given initial particle flux could potentially carry at given absolute values of the ion velocities. More specifically,

$$\eta_T = \left[\int f_\infty v_z^2 d^3v d(\pi r^2) \right] \left[\int f_0 v_z v^2 d^3v d(\pi r^2) \right]^{-1}. \quad (60)$$

Both η_p and η_T can be calculated in a straightforward way based on a numerical solution of Eqs. (17)–(19). In addition to the asymptotic expressions (59) and (60), it is also useful to calculate similar quantities for intermediate axial locations; i.e., to replace f_∞ by the local distribution function f . This modification transforms η_p and η_T into functions of z . Figure 6 presents the plots of $\eta_p(z)$ and $\eta_T(z)$ for the nozzle with the parameters of Fig. 4. For comparison, Fig. 6 shows the result from the simulation with a different ion energy of $\varepsilon_i = 100$ eV. The actual efficiencies are the asymptotic values of $\eta_p(z)$ and $\eta_T(z)$, whereas the transient behavior of η_p and η_T can be viewed as an indicator of whether the flow is already detached at a given axial location.

VI. DDEX SIMULATION

In this section, we present simulation results for the conditions of the Detachment Demonstration Experiment (DDEX).⁹ The DDEX facility was specifically designed to examine plasma behavior in a magnetic nozzle and directivity of the plasma plume. The incoming plasma is created by a source in a strong guiding magnetic field. The plasma expands into a vacuum chamber with a diverging magnetic field formed by external coils. One of the plasma sources in DDEX is a washer-stack gun operating at 300 kW in a pulsed regime. It produces an argon plasma with a maximum

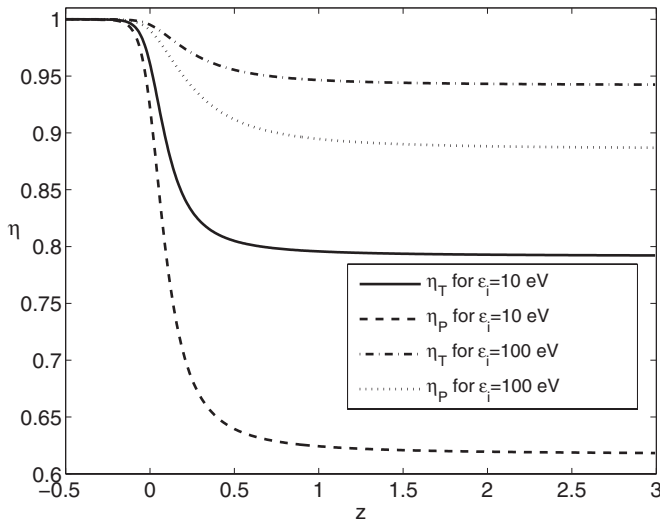


FIG. 6. Intermediate values of the power and thrust efficiencies along the flow (dashed and solid lines) for the nozzle with the parameters of Fig. 4. The dotted and dash-dotted lines show $\eta_P(z)$ and $\eta_T(z)$, respectively, for $\epsilon_i=100$ eV, instead of $\epsilon_i=10$ eV, for the same setup.

density of about 10^{20} m^{-3} and with $\epsilon_i \approx 2$ eV, where ϵ_i is the characteristic ion energy in the flow. The magnetic field in the source is of the order of 0.1 T, so that the flow produced by the source is sub-Alfvénic. The length of the pulse (3 ms) exceeds the ion travel time through the vacuum chamber by an order of magnitude. This allows the flow to reach a steady-state regime during the pulse. The interferometer measurements^{9,10} reveal that the plasma density is indeed roughly constant for about 3 ms.

The plasma density profile measured at 1.87 m downstream from the plasma source is shown in Fig. 7.¹⁷ The dash-dotted line shows the density value that would correspond to a flow with measured incoming density moving strictly along the magnetic field lines produced by the exter-

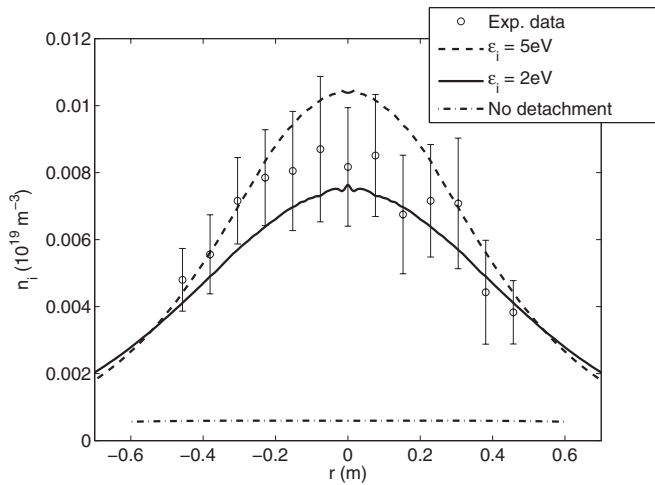


FIG. 7. Measured and calculated radial profiles of the plasma density in DDEX. The circular markers with the corresponding error bars are the experimental data points (Ref. 17). The density value calculated under the assumption that the flow does not affect the magnetic field configuration is shown with a dash-dotted line. The solid and dotted lines are the numerical simulation results for $\epsilon_i=2$ eV and $\epsilon_i=5$ eV, respectively.

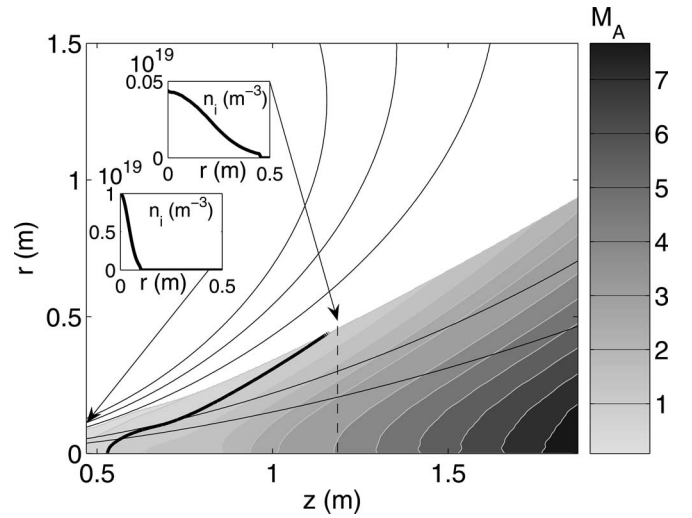


FIG. 8. Simulation results of the plasma plume in DDEX. The contours show the levels of constant Alfvénic Mach number M_A , with the scale indicated on the sidebar. The thick solid line separates the sub- and super-Alfvénic regions. The thin solid lines are the magnetic field lines of the solenoid in the absence of plasma. The insets give radial profiles of n_i in the incoming flow ($z=0.47$ m) and in the plume ($z=1.17$ m).

nal coils without any distortion by the plasma. Clearly, the measured value (circular markers with the corresponding error bars in Fig. 7) is significantly higher. One possible explanation of the large difference between the two density profiles is that the flow stretches the magnetic field lines. This would make the flow cross section smaller and thus the plasma density higher compared to the case where the magnetic configuration remains unaffected by the flow. However, for this explanation to be conclusive, the background gas pressure has to be sufficiently low, so that the ion mean-free-path with respect to charge-exchange collisions is longer than the distance between the plasma source and the location where the plasma density profile is measured. In reality, this requirement is only marginally satisfied in the DDEX facility, which introduces an uncertainty in the interpretation. Nevertheless, it is still appropriate to pose the question of whether the field stretching mechanism alone can account for the observed high density in the plume. In order to answer this question, we carried out a simulation using the procedure described in Sec. IV.

We use the experimentally measured density at 0.47 m downstream from the source as an incoming flow in our calculations. The radial density profile is approximated by a Gaussian profile with $n=n_0 \exp(-r^2 \ln 2 / \sigma^2) H(r_p-r)$, where $n_0=10^{19} \text{ m}^{-3}$ is the peak density at 0.47 m, $\sigma=0.0465$ m is the profile half-width, $r_p=0.093$ m is the plasma radius, and H is the Heaviside step-function. The vacuum field at the plasma boundary is precalculated using the actual coil configuration of DDEX.

Figure 8 shows the Alfvénic Mach number for the 2 eV ions. The ions were assumed to have no gyroenergy. We observe that the initially sub-Alfvénic incoming flow becomes super-Alfvénic downstream. The divergence of the plasma flow is significantly less than the divergence of the

magnetic field lines calculated in the absence of plasma (thin solid lines in Fig. 8).

The calculated radial density profile at 1.87 m downstream from the source is shown in Fig. 7 with a solid line. The density increase due to the magnetic field stretching is comparable to the increase observed in the experiment. For comparison, Fig. 7 also shows a density profile that would correspond to 5 eV ions. We can see that, despite some difference between the 2 and 5 eV profiles, both of them fall in the range of the experimental data.

VII. CONCLUSIONS

We have presented a physics-based numerical model to evaluate efficiency of plasma detachment from a magnetic nozzle for a given supersonic (but sub-Alfvénic) incoming flow. Motivated by the needs of the VASIMR project, this model involves two important approximations relevant to high-power plasma thrusters. First, the choice of supersonic incoming flow enables us to safely neglect any effects associated with electron pressure and the ambipolar electric field. The problem thus reduces to dealing with a charge-neutralized ion flow in a self-consistently determined magnetic field. Second, the practical need for the nozzle to be efficient gives strong preference to slowly diverging flows with paraxial magnetic field inside the plasma, which brings significant technical simplifications into our description of a steady-state flow.

Direct solution of a steady-state problem, as opposed to an initial value problem, eliminates the need to deal with transient phenomena that are of secondary importance for continuously operating plasma thrusters. The steady-state formulation of the problem is also advantageous in terms of computational requirements, which makes the presented model suitable for exploring a range of plasma parameters and magnetic coil configurations needed to design an optimum nozzle. We envision that this detachment-oriented code can serve as a module in an integrated model of a thruster, which would include modeling of plasma production and its acceleration to supersonic velocities.

By considering a given supersonic input, we separate the detachment issue from the problem of creating such an input

flow. The latter typically requires a magnetic mirror that plays the role of the nozzle throat in the conventional gas-dynamic de Laval nozzle. The transition from sub- to supersonic flow occurs due to electron pressure and ambipolar acceleration of the ions. It is noteworthy that electron kinetics is a quite nontrivial part of the problem because the commonly used Boltzmann distribution does not properly describe the collisionless electrons downstream from the magnetic mirror. This aspect will be discussed in detail in a recently completed separate paper.

ACKNOWLEDGMENTS

This work is supported by Ad Astra Rocket Company and the U.S. Department of Energy under Contract No. DE-FG02-04ER-54742. The authors thank R. D. Bengtson, J. Meyers, D. G. Chavers, C. C. Dobson, J. E. Jones, B. M. Schuettepelz, and C. Deline for providing experimental data and for stimulating discussions.

¹See National Technical Information Service Document No. DE00763033 (R. A. Gerwin, G. J. Marklin, A. G. Sgro, and A. H. Glasser, LANL, Los Alamos, NM, AFOSR Technical Report AL-TR-89-092, 1990). Copies may be ordered from National Technical Information Service, Springfield, VA.

²R. W. Moses, R. A. Gerwin, and R. A. Schoenberg, *AIP Conf. Proc.* **246**, 1293 (1992).

³E. B. Hooper, *J. Propul. Power* **9**, 757 (1993).

⁴A. V. Arefiev and B. N. Breizman, *Phys. Plasmas* **12**, 043504 (2005).

⁵E. Parker, *Astrophys. J.* **128**, 664 (1958).

⁶F. R. Chang-Díaz, *Sci. Am.* **283**, 90 (2000).

⁷A. V. Arefiev and B. N. Breizman, *Phys. Plasmas* **11**, 2942 (2004).

⁸B. N. Breizman and A. V. Arefiev, *Phys. Plasmas* **8**, 907 (2001).

⁹D. G. Chavers, C. Dobson, J. Jones, M. Lee, A. Martin, J. Gregory, J. Cecil, R. D. Bengtson, B. Breizman, A. Arefiev, F. Chang-Díaz, J. Squire, T. Glover, G. McCaskill, J. Cassibry, and Z. Li, *AIP Conf. Proc.* **813**, 465 (2006).

¹⁰R. D. Bengtson, private communication (2006).

¹¹R. Winglee, T. Ziemba, L. Giersch, J. Prager, J. Carscadden, and B. R. Roberson, *Phys. Plasmas* **14**, 063501 (2006).

¹²T. M. York, B. A. Jacoby, and P. Mikellides, *J. Propul. Power* **8**, 1023 (1992).

¹³M. Tanaka and I. Kimura, *J. Propul. Power* **4**, 428 (1988).

¹⁴D. V. Sivukhin, in *Reviews of Plasma Physics*, edited by M. A. Leontovich (Consultants Bureau, New York, 1965), Vol. 1, p. 1.

¹⁵K. Yee, *IEEE Trans. Antennas Propag.* **14**, 302 (1966).

¹⁶P. Bogacki and L. F. Shampine, *Appl. Math. Lett.* **2**, 1 (1989).

¹⁷Private communications with the DDEX experimental team (2007).